PHYSICAL REVIEW C VOLUME 36, NUMBER 4 OCTOBER 1987

# Fusion evaporation and fusion-fission with aligned $^{23}$Na ions at energies near and below the fusion barrier

R. Butsch,* H. Jänsch, D. Krämer, K.-H. Möbius,† W. Ott, E. Steffens, G. Tungate,‡ and A. Weller§
*Max-Planck-Institut für Kernphysik, D-6900 Heidelberg, Federal Republic of Germany*

K. Becker, K. Blatt, H. Leucker, W. Luck, and D. Fick
*Philipps Universität, Fachbereich Physik, D-3550 Marburg, Federal Republic of Germany*

P. Paul
*Department of Physics, State University of New York at Stony Brook, Stony Brook, New York 11794*
(Received 28 May 1987)

Using aligned $^{23}$Na beams, fusion cross sections $\sigma^{\text{fus}}$ and second-rank tensor analyzing powers for fusion $T_{20}^{\text{fus}}$ have been measured at energies near and below the fusion barrier for $^{23}\text{Na}+^{48}\text{Ti}$ and for $^{23}\text{Na}+^{206}\text{Pb}$. At sub-barrier energies, large, nearly maximal, values of $T_{20}^{\text{fus}}$ occur, especially for fusion with the heavy target $^{206}$Pb. This reflects the strong influence of the spectroscopic deformation of the projectile on the fusion process at energies below the barrier. However, within a quantum-mechanical coupled-channels calculation this degree of freedom is not enough to describe both the fusion cross section and the second-rank tensor analyzing power for fusion in the energy regime below the fusion barrier. It is shown that the coupling of the fusion channel to inelastic excitations of the projectile and the target can describe the magnitude and energy dependence of $T_{20}^{\text{fus}}$ for both heavy ion systems, but fails to reproduce the "sub-barrier enhancement" of the fusion cross section for both systems.

## I. INTRODUCTION

At energies near the fusion barrier the cross section for the formation of an equilibrated compound system is determined by the properties of the entrance channel, which is often characterized by a one-dimensional barrier. In such a model fusion cross sections are obtained by calculating transmission coefficients with a real, local nuclear interaction potential according to a Wentzel-Kramers-Brillouin (WKB) or Hill and Wheeler formalism,[1] for which the distance between projectile and target is the only variable. These models work well for light $1p$ shell nuclei.[2] However, the measured cross section for fusion of more massive heavy ions is enhanced by several orders of magnitude at sub-barrier energies compared to this type of one-dimensional calculation.[3] It is now well established for such systems that coupling of additional degrees of freedom to the one-dimensional motion is essential for a description of the dynamics of the fusion process at sub-barrier energies.

Many additional degrees of freedom have been considered, including the influence of static deformation, effects of zero point fluctuations of the surface of the colliding nuclei, coupling to low lying excited states of the projectile and the target, and coupling to transfer channels.[2,3] Any kind of coupling results in a splitting of the central potential height, thus producing an eigenvalue spectrum of barriers.[4] Since the center of gravity of this spectrum of barriers has to coincide with the unsplit barrier, some of the new eigenvalues are lower than the unsplit barrier, which leads to an enhancement of the cross section for fusion at sub-barrier energies.

New independent information about the nature of the coupling leading to the enhancement is obtained by studying the sub-barrier fusion process using aligned projectiles. Previous experiments using aligned light ions, such as $^6$Li and $^7$Li, have shown that fusion cross sections obtained with aligned projectiles are influenced strongly by the spectroscopic deformation of the projectile.[5] Furthermore, investigations of the sub-Coulomb interaction of aligned $^7$Li nuclei with various targets revealed the excitation of the aligned projectile as an important part of the interaction.[6] Both phenomena are expected to play an essential role in the understanding of the sub-barrier fusion mechanism. It seems therefore worthwhile and promising to investigate the fusion process at energies below the barrier with aligned heavy ions.

Such experiments with heavy ions are now performed at Heidelberg with a polarized $^{23}$Na beam.[7] The additional observable in fusion reactions initiated by aligned projectiles is the second-rank tensor analyzing power for fusion $T_{20}^{\text{fus}}$ which measures the sensitivity of the fusion process to the alignment of the beam.

The projectile $^{23}$Na has a ground state nuclear spin $I=\frac{3}{2}$. For a $^{23}$Na beam prepared in a nuclear magnetic substate $m$ the fusion cross section is given by[8]

$$\sigma_m^{\text{fus}}=\sigma^{\text{fus}}[1+t_{20}(m)T_{20}^{\text{fus}}] .$$

$\sigma^{\text{fus}}$ denotes the fusion cross section obtained with an unpolarized beam and $t_{20}(m)$ is the alignment of the beam. Using $^{23}$Na beams with two different alignments $t_{20}$ $(m=\frac{3}{2})$ and $t_{20}$ $(m=\frac{1}{2})$, the tensor analyzing power

 

for fusion can be expressed as

$$T_{20}^{\mathrm{fus}} = \frac{1}{|t_{20}|} \frac{\sigma_{m=3/2}^{\mathrm{fus}} - \sigma_{m=1/2}^{\mathrm{fus}}}{\sigma_{m=3/2}^{\mathrm{fus}} + \sigma_{m=1/2}^{\mathrm{fus}}} \quad . \tag{1}$$

In deriving Eq. (1) it is assumed that

$$t_{20}(m=\tfrac{3}{2}) = -t_{20}(m=\tfrac{1}{2}) =: |t_{20}| \ ,$$

which is a reasonable assumption supported by investigations of depolarization mechanisms during the acceleration of the polarized $^{23}$Na beam[9] (see Sec. II D).

The alignment of the nuclear spin of $^{23}$Na also implies the alignment of its (positive) spectroscopic nuclear quadrupole moment. Thus, by measuring the fusion process for different magnetic substates $m$ one measures the cross section for fusion for the two shape orientations $m=\frac{3}{2}$ and $m=\frac{1}{2}$.

We studied the sub-barrier fusion of two heavy ion systems, $^{23}$Na+$^{48}$Ti and $^{23}$Na+$^{206}$Pb:

(i) These targets were chosen to probe systems with a large difference in their Coulomb energies.

(ii) Both targets have a $J^{\pi}=0^{+}$ ground state nuclear spin and a first excited $2^{+}$ state at $\approx 1$ MeV; therefore, the same level scheme for the coupled-channels formalism could be used for both systems.

(iii) All ground state $Q$ values for one- and two-particle transfer are negative for $^{23}$Na+$^{48}$Ti, whereas for $^{23}$Na+$^{206}$Pb both positive and negative ground state $Q$ values are present, which allows one to learn about the influence of transfer channels.

## II. EXPERIMENT

### A. General

The experiments were performed with aligned $^{23}$Na ions produced by the atomic beam source for polarized heavy ions at the Max-Planck Institut für Kernphysik at Heidelberg.[7] By means of conventional atomic beam techniques[10] and laser optical pumping[9] this source produces polarized $^{23}$Na$^{-}$ ions predominantly ($\approx 90\%$) in a single nuclear $m$ substate. Using a high frequency transition[11] the population of the atomic beam was switched frequently (frequency $\approx 2$ Hz) between the $m=\frac{3}{2}$ and $m=\frac{1}{2}$ magnetic substates to reduce systematic errors in the determination of $T_{20}^{\mathrm{fus}}$. In a fusion experiment the beam axis is the only uniquely defined axis and is the natural quantization axis for these experiments. Nuclear magnetic substate populations relative to this quantization axis were maintained through proper adjustment of the electromagnetic fields in a Wien filter at the ion source.

Polarized ions from the ion source were accelerated in an MP tandem. To avoid depolarization by hyperfine interaction during the transport to the target, it is necessary that ions be transported with a spin zero electronic shell or fully stripped.[9] At the highest energy of the MP tandem, the stripping probability into the $11^{+}$ charge state is less than $10^{-4}$. Therefore, $^{23}$Na ions stripped to the $9^{+}$ charge state in the tandem terminal were selected for the experiments, which is a compromise between a reasonable stripping probability ($\approx 2-3\%$) and tolerable nuclear depolarization (around 50%).[9]

The choice of this charge state and the requirement of maximum intensity fix the beam energy of $^{23}$Na$^{9+}$ ions leaving the MP tandem in a narrow energy range from about 90 to 120 MeV. To perform experiments with polarized $^{23}$Na ions without this energy restriction, a post-accelerator following the MP tandem was used to accelerate or decelerate the beam to the desired energies. Since the $s$-wave fusion barriers for the two systems under investigation are predicted from barrier systematics[12] at beam energies of about 50 MeV ($^{23}$Na+$^{48}$Ti) and 111 MeV ($^{23}$Na + $^{206}$Pb), the post-accelerator was used to decelerate the beam for the $^{23}$Na + $^{48}$Ti fusion experiment. During the deceleration process no further depolarization of the nuclear spin was observed.[9]

### B. Fusion evaporation: $^{23}$Na+$^{48}$Ti

Targets of 50 $\mu$g/cm$^2$ $^{48}$Ti on carbon backing (10 $\mu$g/cm$^2$, 20 $\mu$g/cm$^2$ $^{12}$C) were bombarded with aligned $^{23}$Na ions at $E_{\mathrm{lab}}=48.0$, 49.5, 52.0, 54.0, 56.6, 63.0, 67.3, and 72.5 MeV and with an unpolarized $^{23}$Na beam[13] at $E_{\mathrm{lab}}=50$, 55, 60, 63, and 66 MeV. Typical beam currents were 0.5–2 nA. For the $^{23}$Na+$^{48}$Ti system at these low energies we assume that the fusion cross section is given by the evaporation residue cross section.

In the energy range of the experiment evaporation residues are produced with mean kinetic energies ranging from 15.5 to 23.5 MeV. The evaporation residues were identified by time-of-flight technique. A rebuncher resonator was used in conjunction with the pulsing system of the MP tandem accelerator to generate subnanosecond beam pulses at the target[14] with a repetition period of 74 ns. A corresponding signal served as start signal for the time-of-flight measurement. The stop signal and therefore the time of flight $t$, was obtained from Si surface barrier detectors (100–250 $\mu$m thickness) which also measured the energy $E$ of the reaction products. Seven detectors were placed in a plane at positions of $\vartheta_{\mathrm{lab}}=3°$, 4°, 7.5°, 11°, 14.5°, 18°, and 21.5° with respect to the beam axis. (In the first run of the experiment the most forward angle was only 4°.) Two detectors at $\vartheta_{\mathrm{lab}}=0°$, but $\pm 5°$ out of plane, were used to detect any offset of the beam with respect to the detector plane. A short flight distance of 20–25 cm was chosen to increase the detection efficiency for evaporation residues at the expense of their mass resolution. The geometric solid angles of the detectors were in the range of 0.1–7.5 msr as verified by calibration with an $^{241}$Am $\alpha$ source. For the purpose of fast timing signals the detectors were cooled to $-20$ °C. The time calibration and time resolution of the detector system were established by elastically scattered $^{23}$Na ions from a thin 50 $\mu$g/cm$^2$ $^{197}$Au target. The time resolution (FWHM) was measured to be $\approx 100$ ps at the highest bombarding energies, but rose to $\approx 350$ ps at the lowest bombarding energy.

The mass $m$ of all reaction products was calculated from the relation $m \propto Et^2$, and in the energy versus mass spectrum shown in Fig. 1(a), the evaporation residues are clearly separated from other reaction products. Eva-

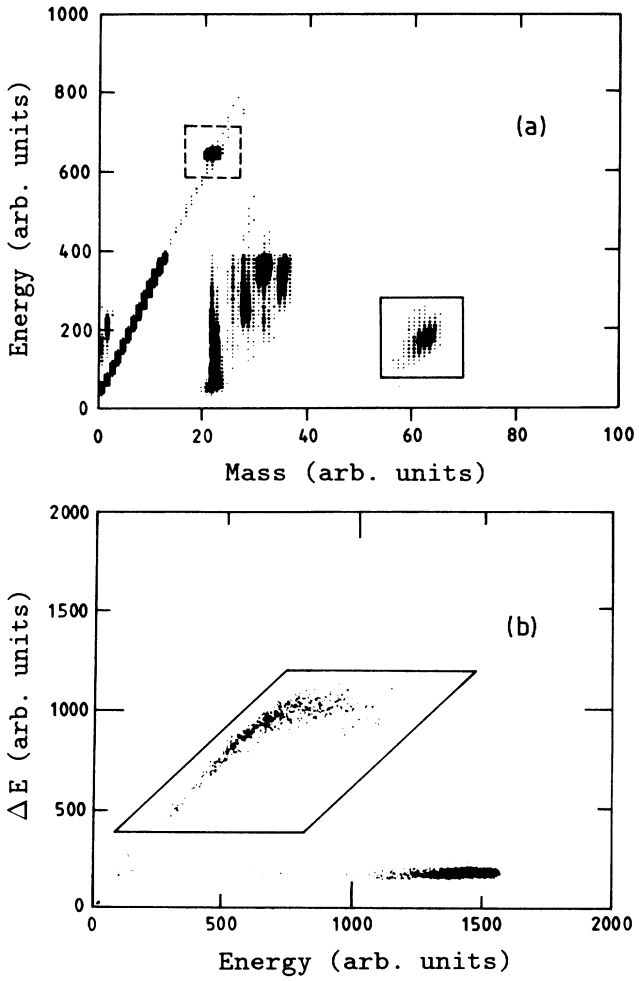


FIG. 1. (a) Energy versus mass spectrum of the reaction $^{23}$Na + $^{48}$Ti at $E_{lab}=66$ MeV and $\vartheta_{lab}=4.2°$. Fusion events are enclosed by the solid line, elastically scattered particles by the dashed line. (b) $\Delta E$-$E$ plot of the $^{23}$Na+$^{206}$Pb reaction at $E_{lab}=120$ MeV and $\vartheta_{lab}=94.7°-106.0°$. The fission events are in the region of high $\Delta E$ enclosed by the solid line.

poration residues from reactions with $^{48}$Ti are in the region of low energy and high mass (solid box). Elastically scattered particles are in the region of high energy (dashed box). Between these two regions lie evaporation residues from fusion reactions with carbon and other contaminants in the target.

### C. Fusion-fission: $^{23}$Na+$^{206}$Pb

A 100 $\mu$g/cm$^2$ $^{206}$Pb target (enriched to 97.39±0.05 %) on a 15 $\mu$g/cm$^2$ $^{12}$C backing was bombarded with aligned $^{23}$Na ions at laboratory energies of $E_{lab}=108$, 111, 114, 117, and 120 MeV with beam currents between 10 and 20 nA. As will be discussed at the end of this subsection, fission of the compound nucleus $^{229}$Np is the dominant fusion decay channel. The fission fragments were identified with four $\Delta E-E$ telescopes. These were placed about the beam axis in the backward hemisphere covering the angles 73.6°–89.0°, 94.7°–106.0°, 132.6°–150.0°, and 147.7°–159.7°. Each telescope[15] consisted of a gas ionization chamber ($\Delta E$) followed by a 300 $\mu$m thick Si surface barrier ($E$) detector which could be operated in a position sensitive mode. Two position sensitive $E$ detectors were used for angular distributions of the fission fragments and hence fission cross sections, whereas $T_{20}^{fus}$ was measured using all telescopes. The scattering angles were defined by nine and ten slits, respectively (each 7 mm×4 mm) in front of the $E$ detectors. The telescopes were mounted at distances between 14.4 and 20.9 cm from the target. Geometric solid angles defined by the slits in front of the $E$ detectors were in the range of 0.6–1.4 msr. The telescopes were operated at 15 Torr of Ar (90%)-$CH_4$ (10%) to take advantage of the large specific energy loss of fission fragments at this low gas pressure. From the $\Delta E-E$ correlation the fission fragments are clearly identified [solid box in Fig. 1(b)]. The increasing energy loss of the fission fragments with increasing energy occurs because the energy loss of the fission fragments is less than the corresponding Bragg maximum. A monitor counter installed at $\vartheta_{lab}=18°$ was used for an absolute normalization of the cross section.

Prior to an identification of the fission yield with the fusion cross section, one should question whether fission is the only open fusion decay channel in the $^{23}$Na +$^{206}$Pb reaction, and whether there are other processes contributing to the observed fission yield.

(i) Formation of evaporation residues is negligible for the heavy ion system $^{23}$Na+$^{206}$Pb. This can be concluded from systematics[16] and from calculations using the Monte Carlo evaporation code JULIAN/PACE2 (Ref. 17) with default parameters.

(ii) Fission after transfer reactions is also negligible in the measured energy range because the fission barriers in the mass region of lead are high (see, e.g., Ref. 18).

(iii) Deep inelastic reactions are expected to play no role at barrier energies.

(iv) At most, small contributions to the fission yield from "quasifission" are expected.[19]

Thus, for the $^{23}$Na+$^{206}$Pb reaction in the measured energy range, fission is the predominant fusion decay channel, and in the following we assume $\sigma^{fus}=\sigma^{fission}$.

### D. Polarimeters

For the two experiments two different types of polarimeters had to be used to determine the alignment $t_{20}$ of the $^{23}$Na beam. The polarimeters were installed downstream of the detector arrangement for the respective fusion experiment. For an absolute calibration of the alignment $t_{20}$, the targets ($^{48}$Ti/$^{206}$Pb) were removed from the beam to avoid depolarization through hyperfine interaction. However, with the target in the beam the polarimeter could still be used to monitor changes in the alignment of the $^{23}$Na beam during the fusion experiment. The experimental value of $t_{20}$ was obtained from

$$|t_{20}| = \frac{1}{T_{20}} \frac{N_{m=3/2}-N_{m=1/2}}{N_{m=3/2}+N_{m=1/2}} . \quad (2)$$

Thus, the counting rate $N_m$ of a specific "polarimeter reaction" of a known tensor analyzing power $T_{20}$ yields the alignment $t_{20}$. A systematic uncertainty in the determination of the beam alignment may result if $t_{20}$ $(m=\frac{3}{2}) \neq -t_{20}$ $(m=\frac{1}{2})$, i.e., if the unpolarized part in the beam is different for different alignments $t_{20}$ $(m=\frac{3}{2})$ and $t_{20}$ $(m=\frac{1}{2})$ (see also Sec. I). However, the deviation is estimated to be small ($\approx 2\%$) for a $^{23}$Na beam at the exit of the ion source, and it is not expected that this deviation will be enlarged during the transport to the target.[9] Moreover, in the tensor analyzing power for fusion, $T_{20}^{\mathrm{fus}}$, this uncertainty will cancel in first order.

For the energies of the $^{23}$Na+$^{48}$Ti experiment Coulomb excitation of $^{23}$Na to its first excited state at $E^*=0.44$ MeV served as a "polarimeter reaction." The cross section for this reaction depends on the alignment of the $^{23}$Na beam and the tensor analyzing power $T_{20}^{\mathrm{Coul\,ex}}$, which can be calculated accurately.[20] When $^{208}$Pb is used as a polarimeter target, one calculates a maximum tensor analyzing power of $T_{20}^{\mathrm{Coul\,ex}}$ ($^{208}$Pb)=0.65 at backward angles, nearly independent of the bombarding energies. Since the cross section for Coulomb excitation decreases with decreasing energy, a $^{90}$Zr target rather than a $^{208}$Pb target was used at the lowest energies to obtain reasonable counting rates [$T_{20}^{\mathrm{Coul\,ex}}$($^{90}$Zr)=0.66 at backward angles]. The polarimeter[21] consists of a position sensitive ring parallel plate avalanche counter covering an angular range from 134° to 169° and two NaI counters placed at ±90° with respect to the beam axis. Backscattered $^{23}$Na ions were detected in coincidence with $\gamma$ rays ($E_\gamma=0.44$ MeV). From the counting rates $N_m^{\mathrm{Coul\,ex}}$ for both magnetic substates, the alignment $t_{20}$ was calculated using Eq. (2). The experimental results obtained for different beam energies were $t_{20}=0.41\pm0.05$ ($E_{\mathrm{lab}}=52.0$, 56.6, 63.0, 67.3, and 72.5 MeV), $t_{20}=0.41\pm0.03$ ($E_{\mathrm{lab}}=54.0$ MeV), $t_{20}=0.46\pm0.04$ ($E_{\mathrm{lab}}=49.5$ MeV), and $t_{20}=0.48\pm0.10$ ($E_{\mathrm{lab}}=48.0$ MeV).

For the $^{23}$Na + $^{206}$Pb experiment the polarimeter described above can no longer be used, because in the energy regime of 108 to 120 MeV nuclear interactions become important and the tensor analyzing power cannot be calculated model independently. We therefore chose the $^1$H($^{23}$Na,$^4$He)$^{20}$Ne(g.s.) reaction which, at zero degrees, has an energy independent tensor analyzing power[22] of $T_{20}=-1$. The polarimeter consisted of a 480 $\mu$g/cm$^2$ $(CH_2)_n$ foil followed by a 30 $\mu$m Ta foil and a Si surface barrier detector at zero degrees. The alignment of the beam was measured only at 110 MeV bombarding energy. After passing through the polarimeter target the beam was stopped in the Ta foil. The $\alpha$ particles passed through the Ta foil and were detected with the Si surface barrier detector, giving yields $N_m^\alpha$ for both magnetic substates. From Eq. (2) the alignment $t_{20}$ was calculated to be $t_{20}=0.39\pm0.03$. This value was used throughout the fusion-fission experiment.

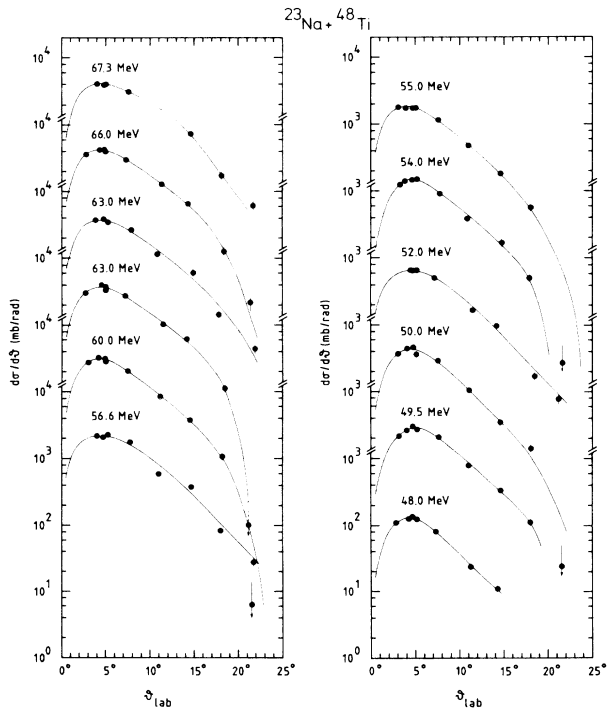


FIG. 2. Angular distributions $d\sigma/d\vartheta$ for evaporation residues of $^{23}$Na+$^{48}$Ti fusion at various bombarding energies. The solid curves are polynomial fits to the data as explained in the text.

## III. EXPERIMENTAL DATA

### A. Angular distributions

For the analysis of the $^{23}$Na+$^{48}$Ti experiment, two-dimensional $E$ vs $m$ spectra were produced for both magnetic substates to obtain the yield of evaporation residues and of elastically scattered particles at angle $\vartheta_{\mathrm{lab}}$ [see Fig. 1(a)]. To compute angular distributions for unpolarized projectiles the yields for both magnetic substates were summed. Angular distributions $d\sigma^{\mathrm{fus}}/d\Omega_{\mathrm{lab}}$ were obtained by normalizing the yield of the evaporation residues at each angle to the yield of elastically scattered particles at forward angles, where Rutherford scattering was assumed. The yield of elastically scattered particles was corrected for target contaminants ($^{12}$C backing, $^{16}$O, $^{24}$Mg, and $^{181}$Ta/$^{232}$Th) whose contributions could be determined by elastic scattering at larger angles ($\vartheta_{\mathrm{lab}}>18°$). The normalization procedure included the correction of the scattering angles for any horizontal and/or vertical offset of the beam with respect to 0°. The cross section for Rutherford scattering was averaged over the opening angles of the detectors used for normalization, and the energy of the beam was corrected to the energy at the middle of the target.

To obtain the total fusion cross section the angular distributions $d\sigma^{\mathrm{fus}}/d\Omega_{\mathrm{lab}}$ were fitted with polynomials and then transformed to $d\sigma^{\mathrm{fus}}/d\vartheta_{\mathrm{lab}}$. This representation makes the extrapolation to $\vartheta_{\mathrm{lab}}=0°$, and thus the angle integration, more accurate. Figure 2 shows the angular distributions together with polynomial fits (solid lines). The shape of the angular distributions of the evaporation residues does not change much over the measured energy range. The increased evaporation of parti-

cles with increasing energy broadens the angular distributions, but this tendency is offset by a forward focusing of the evaporation residues resulting from the larger recoil velocity of the compound nucleus.

The fission fragment angular distributions for the $^{23}Na + {}^{206}Pb$ reaction were obtained by integrating the fission events in the $\Delta E$ spectra for each angle defined by the slits in front of the position sensitive $E$ detectors. This yield was divided by 2 because the experiment does not distinguish between the two fission fragments. The yield was then normalized at each angle to the yield of elastically scattered particles measured in the forward monitor detector. The contribution of contaminants in the $^{206}Pb$ target ($^{12}C$ backing, $^{16}O$) to the yield of elastically scattered particles in the monitor detector at $\vartheta_{lab}=18°$ is negligible, because the grazing angles for elastic scattering on $^{12}C$ and $^{16}O$ are much less than 18°. However, these contaminants are important for the calculation of the energy loss of the beam in the target. The energy of the beam was again corrected to the midpoint of the target.

The angular distributions $d\sigma^{fus}/d\Omega_{lab}$ were transformed to the center-of-mass system assuming symmetric fission whereby kinetic energies of the fission fragments were calculated from Viola systematics.[23] Angular distributions $d\sigma^{fus}/d\theta_{c.m.}$ were obtained assuming $d\sigma^{fus}/d\Omega_{c.m.}$ to be proportional to $1/\sin\theta_{c.m.}$. Figure 3 displays these angular distributions, which turned out to be independent of the scattering angle $\theta_{c.m.}$ (dashed lines).

### B. Excitation functions

The fusion cross section for $^{23}Na+{}^{48}Ti$ was obtained by integrating the angular distributions $d\sigma^{fus}/d\vartheta_{lab}$ shown in Fig. 2. The fusion cross section for $^{23}Na+{}^{206}Pb$ was calculated using

$$\sigma^{fus}=\pi\langle d\sigma^{fus}/d\theta_{c.m.}\rangle ,$$

where the $\langle d\sigma^{fus}/d\theta_{c.m.}\rangle$ are the weighted mean values of $2\pi\sin\theta_{c.m.}d\sigma^{fus}/d\Omega_{c.m.}$ indicated by the dashed lines in Fig. 3.

The tensor analyzing power for fusion, $T_{20}^{fus}$, was determined in the following way. For the $^{23}Na+{}^{48}Ti$ system, the yields of evaporation residues from all detectors identified in the two-dimensional $E$ vs $m$ spectra were summed for each magnetic substate separately, yielding $N_{m=3/2}^{fus}$ and $N_{m=1/2}^{fus}$. For $^{23}Na+{}^{206}Pb$ the fusion-fission yield was extracted from the angle integrated $\Delta E$ spectrum of each telescope. The yields from all telescopes

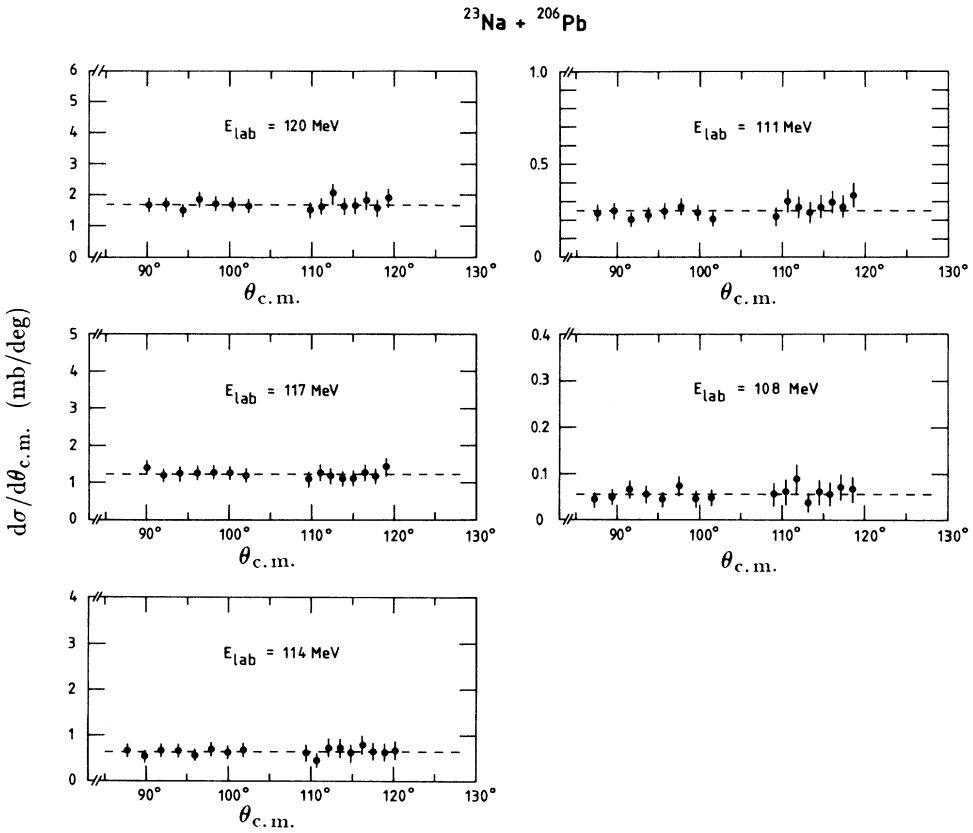


FIG. 3. Angular distributions $d\sigma/d\theta_{c.m.}$ for fission fragments from $^{23}Na + {}^{206}Pb$ interaction at various bombarding energies.

were summed to obtain the total fusion yield $N_m^{\rm fus}$ for each magnetic substate. The experimental value of $T_{20}^{\rm fus}$ can then be calculated from Eq. (2) using the $t_{20}$ values listed in Sec. II D.

The excitation functions of the fusion cross section and the tensor analyzing power for fusion are shown in Fig. 4 for both systems together with results from calculations which are described in Sec. V. For both systems $\sigma^{\rm fus}$ displays the typical strong energy dependence of fusion cross sections near the fusion barrier (33.4 MeV for $^{23}$Na+$^{48}$Ti, 99.5 MeV for $^{23}$Na+$^{206}$Pb; see Sec. IV A). $T_{20}^{\rm fus}$ shows a strong energy dependence as well. Values of $T_{20}^{\rm fus}$ are small at high energies and rise to large and positive values at energies near and below the barrier. [Recall that $T_{20}^{\rm fus}$ is bounded by $\pm 1$ according to Eq. (1).] At low energies the sign of $T_{20}^{\rm fus}$ is positive and opposite to the sign observed for fusion of aligned $^7$Li nuclei.[5] This indicates the strong influence of the spectroscopic deformation of the aligned projectile on the fusion process at sub-barrier energies. The sign of $T_{20}^{\rm fus}$ at barrier energies is directly connected to the sign of the spectroscopic quadrupole moment of the aligned projectile: the spectroscopic quadrupole moment is positive for $^{23}$Na ($Q_S = +10.06\ e\ {\rm fm}^2$, Ref. 24) and negative for $^7$Li ($Q_S = -3.7\ e\ {\rm fm}^2$, Ref. 6). In this context it is worthwhile to note that for the lowest measured energy in the $^{23}$Na+$^{206}$Pb system ($T_{20}^{\rm fus} \approx 0.8$) almost 90% of the total cross section for fusion results from the $m = \frac{3}{2}$ component in the beam.

The uncertainty in $T_{20}^{\rm fus}$ results from the statistical error of the fusion yield and from the uncertainty in the determination of the beam polarization. Systematic errors are expected to be small because of the rapid switching between $m$ substates. Statistical uncertainties for $\sigma^{\rm fus}$ are between 5.1% and 13.4% for $^{23}$Na+$^{48}$Ti and between 14.7% and 36% for $^{23}$Na+$^{206}$Pb. The large uncertainty of 36% stems mainly from poor statistics of the fission yield at the lowest bombarding energy. A systematic uncertainty in the $^{23}$Na+$^{206}$Pb analysis results from the laboratory to center-of-mass transformation of the fission fragment angular distributions and the assumption of a $1/\sin\theta_{\rm c.m.}$ distribution. This uncertainty can be estimated[19] to be in the range of 8–11 % depending on the bombarding energy. For the $^{23}$Na+$^{48}$Ti reaction the uncertainty in the absolute scale for $\sigma^{\rm fus}$ is estimated to be small. This was verified by performing calculations with the JULIAN/PACE2 Monte Carlo code[17] using default parameters.

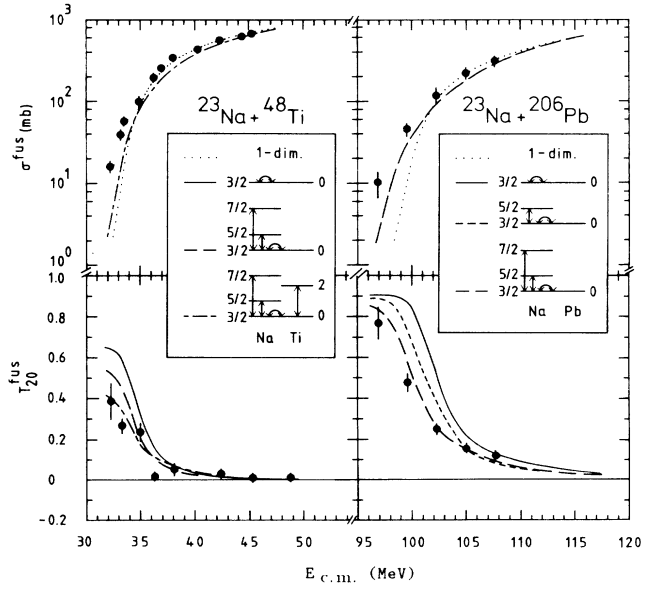


FIG. 4. Cross sections (top part) and tensor analyzing powers (bottom part) for fusion of $^{23}$Na+$^{48}$Ti (left) and $^{23}$Na+$^{206}$Pb (right). The inset shows the coupling schemes used in various quantum-mechanical coupled-channels calculations described in Sec. V. The error bars include only statistical errors.

## IV. ANALYSIS

### A. Nuclear potentials

The excitation functions of the fusion cross section for $^{23}$Na+$^{48}$Ti and $^{23}$Na+$^{206}$Pb were first analyzed with a one-dimensional sharp cutoff model[25] and Wong's formula[26] (without deformation) for the fusion cross section. The one-dimensional $s$-wave barrier parameters obtained from this analysis are collected in Table I. Cross sections computed in these models are compared to the experimental data in Fig. 5. The Wong model contains the quantum-mechanical transmission through the barrier, yielding information about the width $\hbar\omega_B$ of the barrier. To reproduce the fusion cross section at sub-barrier energies within the Wong model (solid lines in the bottom part of Fig. 5) unphysically large values of $\hbar\omega_B$ are needed, in contrast to the prediction of the realistic nuclear potentials discussed below (dashed curve in the bottom part of Fig. 5). For example, the value $\hbar\omega_B = 9.4$ MeV for $^{23}$Na+$^{206}$Pb indicates a very narrow barrier, whereas one expects a broad barrier due to the large Coulomb energy of this system. Clearly, degrees of freedom beyond those accounted for in a one-dimensional ansatz are needed to reproduce the data below the barrier.

To investigate whether inelastic excitation of the projectile and/or target can be identified as these additional degrees of freedom, quantum-mechanical coupled-channels calculations have to be performed. The real and imaginary nuclear potentials entering these calculations must be specified with the constraint that the real part of the nuclear potential, together with the Coulomb potential, has to reproduce the $s$-wave barrier parameters listed in Table I.

To specify the real part of the nuclear potential, the experimental data at above-barrier energies are com-

TABLE I. Barrier parameters for $^{23}$Na+$^{48}$Ti and $^{23}$Na + $^{206}$Pb.

| System | $V_B$ (MeV) | $R_B$ (fm) | $\hbar\omega_B$ (MeV) |
|---|---|---|---|
| $^{23}$Na+$^{48}$Ti | 33.4±0.5 | 9.0±0.3 | 5.7±0.6 |
| $^{23}$Na+$^{206}$Pb | 99.5±1.0 | 11.5±0.5 | 9.4±0.7 |

pared with one-dimensional calculations of the fusion cross section according to

$$\sigma^{\text{fus}}=\frac{\pi}{k^2}\sum_{l=0}^{l_{\max}}(2l+1)T_l \ , \tag{3}$$

$T_l$ being the transmission coefficients in the Hill and Wheeler approximation taking properly into account the $l$ dependence of the barrier parameters $V_B$, $R_B$, and $\hbar\omega_B$. The maximum orbital angular momentum for which a pocket of the central potential exists is given by $l_{\max}$. The central potential is given by

$$V_{\text{centr}}(r,l)=V_{\text{nucl}}(r)+V_{\text{Coul}}(r)+\frac{\hbar^2 l(l+1)}{2\mu r^2} \ ,$$

with

$$V_{\text{Coul}}(r)=Z_P Z_T e^2/r, \quad \text{if } r\geq R_C$$
$$=Z_P Z_T e^2(3R_C^2-r^2)/2R_C^3, \quad \text{if } r\leq R_C \ ,$$

$R_C=1.2(A_P^{1/3}+A_T^{1/3})$ fm, and $\mu$ the reduced mass in the entrance channel. For $V_{\text{nucl}}(r)$, the Woods-Saxon parametrization[27] of the Akyüz and Winther ion-ion folding potential,[28] the Krappe-Nix-Sierk (KNS) potential,[29] and the proximity potential[30] have been considered. The first of these three potentials is given by

$$V_{\text{nucl}}(r)=-16\pi\gamma\frac{R_P R_T}{R_P+R_T}a$$
$$\times\{1+\exp[(r-R_P-R_T)/a]\}^{-1} \ ,$$

with

$$R_i=(1.2A_i^{1/3}-0.09) \text{ fm} \ ,$$
$$1/a=1.17[1+0.53(A_P^{-1/3}+A_T^{-1/3})] \text{ fm}^{-1} \ ,$$

and with

$$\gamma=0.9517\left[1-1.7826\left[\frac{N-Z}{A}\right]^2\right] \text{ MeV/fm}^2 \ ,$$

where $N$, $Z$, and $A$ refer to the compound nucleus. This parametrization reproduces the barrier for the $^{23}$Na+$^{48}$Ti system within the experimental uncertainties but overpredicts it for the $^{23}$Na+$^{206}$Pb system. This is illustrated in Fig. 6, which shows one-dimensional calculations of the fusion cross section according to Eq. (3) without any parameter adjustment.

As expected, these one-dimensional calculations cannot describe the sub-barrier fusion data. For $^{23}$Na +$^{48}$Ti a very good description of the above-barrier data

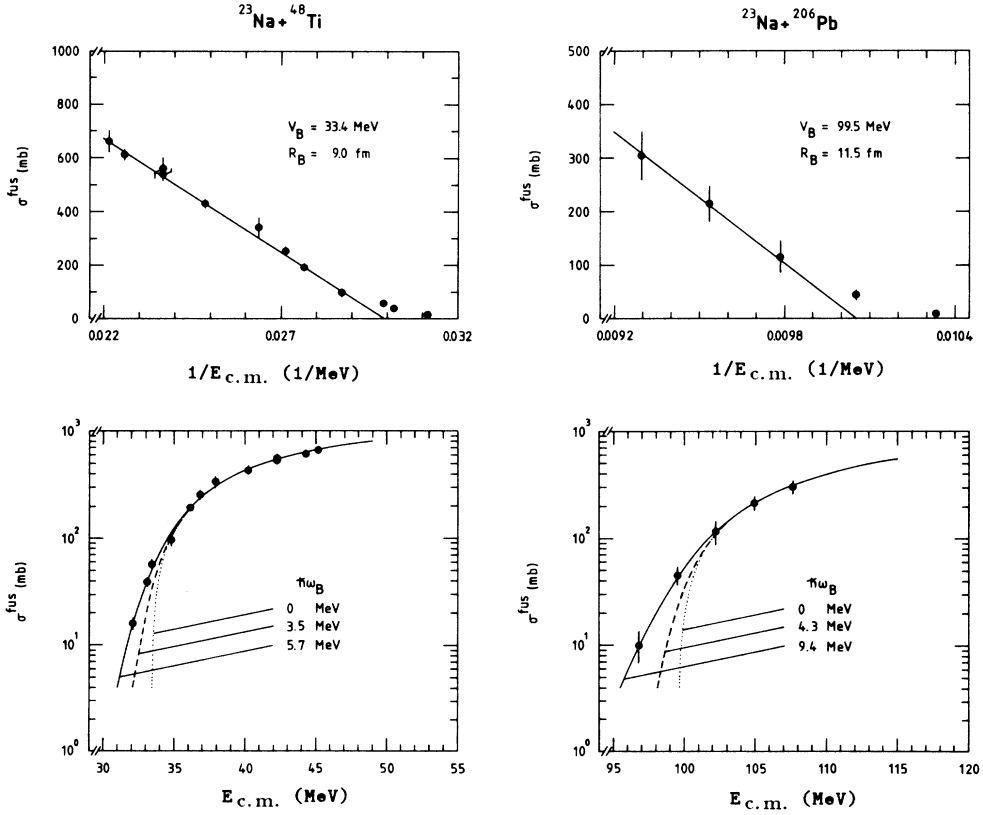


FIG. 5. Fit to the fusion excitation functions with a sharp-cutoff model (upper part, solid curve, and lower part, dotted curve) and Wong's formula (lower part, solid curve). For the sharp cutoff analysis, data points at energies at and below the barrier were neglected. In the lower part the dashed lines are calculated according to Wong using values for $\hbar\omega_B$ obtained with realistic nuclear potentials (see the text).

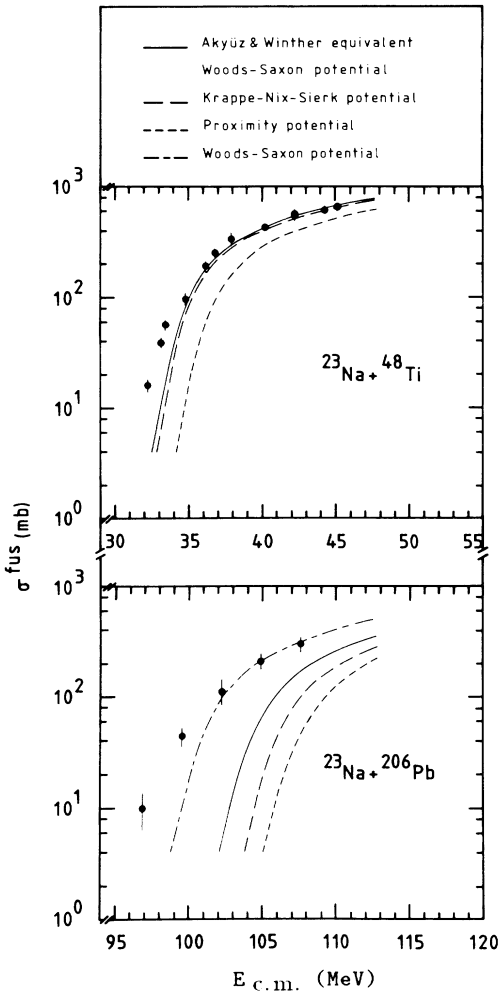


FIG. 6. Predictions for $\sigma^{fus}$ using various nuclear potentials, compared to the data. See the text for further explanation.

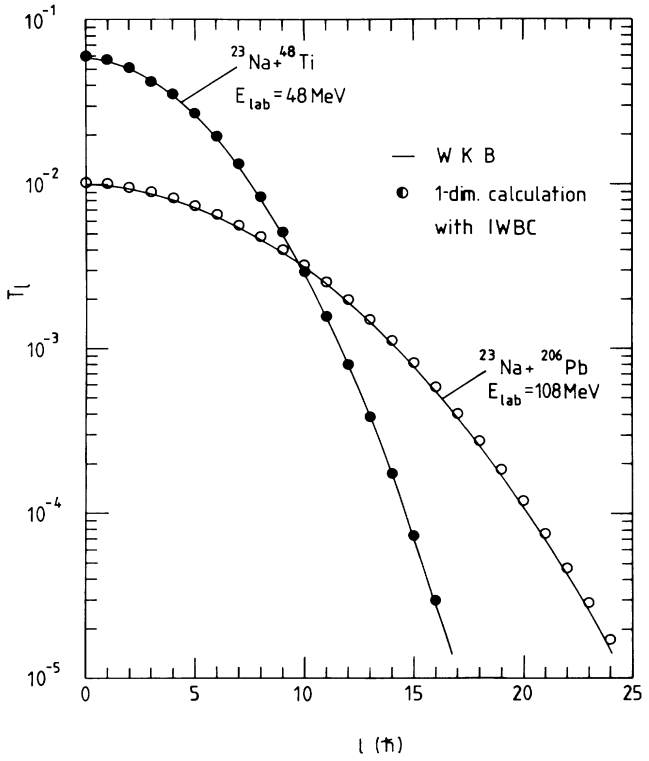


FIG. 7. Comparison of transmission coefficients from WKB and one-dimensional coupled-channels calculations with a short ranged imaginary potential simulating an incoming wave boundary condition (IWBC). The calculations were performed for the lowest bombarding energies.

was obtained with the Woods-Saxon parametrization of the Akyüz and Winther potential given by Broglia and Winther,[27] with parameters (real part) listed in Table II. Also, the KNS potential describes the fusion cross section for $^{23}$Na+$^{48}$Ti at the highest energies. The proximity potential underpredicts the barrier for this system by approximately 1.5 MeV in comparison to the other potentials.

For the heavy system $^{23}$Na+$^{206}$Pb the barrier is overestimated by all potentials. However, a radius change of $\Delta R = 0.3$ fm within the proximity formalism gives satisfactory agreement with the $^{23}$Na+$^{206}$Pb fusion data at above-barrier energies. Similar modifications of the proximity potential have been reported[31] for other heavy ion systems (e.g., $^{16}$O + $^{208}$Pb). We chose a Woods-Saxon form factor for the nuclear potential, and parameters were adjusted to the experimental data at above-barrier energies within their errors (long-dashed–short-dashed curve in the bottom part of Fig. 6). The potential parameters (real part) obtained in this way are also listed in Table II.

For the imaginary part of the nuclear potential a "short range" potential was used to simulate an incoming wave boundary condition.[32] It causes the absorption of those partial waves which tunnel through the barrier. This has been shown to be equivalent to a one-dimensional barrier penetration calculation within a WKB formalism.[32] In this formalism, transmission coefficients are calculated by evaluating the path integral between the inner and outer turning points:

TABLE II. Woods-Saxon parameters for the real and imaginary parts of the nuclear potential used for the coupled-channels calculations.

| | Real part | | Imaginary part | |
|---|---|---|---|---|
| | $^{23}$Na+$^{48}$Ti | $^{23}$Na+$^{206}$Pb | $^{23}$Na+$^{48}$Ti | $^{23}$Na+$^{206}$Pb |
| $V$ (MeV) | 56.8 | 78.0 | 10.0 | 15.0 |
| $R$ (fm) | 7.59 | 10.50 | 7.0 | 10.0 |
| $a$ (fm) | 0.64 | 0.70 | 0.2 | 0.2 |

$$T_l^{\mathrm{WKB}}=\left[1+\exp\left[2\int_{r_{\mathrm{in}}}^{r_{\mathrm{out}}}\left\{\frac{2\mu}{\hbar^2}[V_{\mathrm{centr}}(r,l)-E_{\mathrm{c.m.}}]\right\}^{1/2}\times dr\right]\right]^{-1}.$$

For the imaginary potential a Woods-Saxon parametrization was used and one-dimensional coupled-channels calculations [code ECIS79 (Ref. 33)] with parameters listed in Table II for the real part of the nuclear potential were performed to obtain transmission coefficients calculated from the $S$-matrix elements for elastic scattering according to $T_l=1-|S_l^{\mathrm{elastic}}|^2$. The Woods-Saxon parameters for the imaginary potential were adjusted such as to reproduce the WKB results (Fig. 7). These parameters (imaginary part) are given in Table II.

### B. Theoretical concepts

This subsection shows how the tensor analyzing power for fusion, $T_{20}^{\mathrm{fus}}$, can be obtained within a quantum-mechanical coupled-channels description containing coupling to excited states of the projectile and/or target.

To this end the fusion cross section for each magnetic substate $m$ of the projectile spin must be calculated. We start by defining the fusion cross section as the difference between the total reaction cross section and the cross section for direct reactions restricted here to inelastic excitations

$$\sigma_{\alpha sm}^{\mathrm{fus}}=\sigma_{\alpha sm}^{\mathrm{reaction}}-\sum_{\alpha'}\sum_{s'}\sigma_{\alpha's';\alpha sm}^{\mathrm{inelastic}}\ . \tag{4}$$

Because both targets have a ground state spin of zero, the entrance channel spin $s$ is given by the ground state spin of the projectile $^{23}$Na ($s\equiv I$, thus $m$, the $z$ component of the projectile spin, is equivalent to the $z$ component of the entrance channel spin). The channel spin in the exit channel is denoted by $s'$. The labels $\alpha$ and $\alpha'$ summarize all other quantum numbers in the entrance and exit channel, respectively. Because $\alpha$ and $s$ are fixed, we have $\sigma_m^{\mathrm{fus}}\equiv\sigma_{\alpha sm}^{\mathrm{fus}}$. From the $S$-matrix elements the angle integrated cross section for a reaction $(\alpha sm)\rightarrow(\alpha's')$ is calculated from[34]

$$\begin{aligned}\sigma_{\alpha's';\alpha sm}=\frac{\pi}{k_\alpha^2}\sum_{m'}\sum_{J_1}\sum_{l_1}\sum_{M_1}\sum_{J_2}\sum_{l_2}\sum_{M_2}\sum_{l'}\sum_{\mu'}&\sqrt{2l_1+1}\langle l_1 0sm\mid J_1M_1\rangle\langle l_2 0sm\mid J_2M_2\rangle\\&\times\sqrt{2l_2+1}\langle l'\mu's'm'\mid J_1M_1\rangle\langle l'\mu's'm'\mid J_2M_2\rangle\\&\times(\delta_{\alpha'\alpha}\delta_{s's}\delta_{l'l_1}-S^{J_1}_{\alpha's'l';\alpha sl_1})^*(\delta_{\alpha'\alpha}\delta_{s's}\delta_{l'l_2}-S^{J_2}_{\alpha's'l';\alpha sl_2})\ .\end{aligned}$$

The $S$-matrix elements contain both the Coulomb and the nuclear phases. The orbital angular momenta in the entrance and exit channel are denoted by $l$ and $l'$, respectively. $M$ is the $z$ component of $J$, the total angular momentum; $\mu'$ is the $z$ component of $l'$; and $m'$ is the $z$ component of $s'$. Using an orthogonality relation for the Clebsch-Gordan coefficients one finds:

$$\begin{aligned}\sigma_{\alpha's';\alpha sm}=\frac{\pi}{k_\alpha^2}\sum_J(2J+1)\sum_{l'}\sum_{l_1}\sum_{l_2}&\langle smJ-m\mid l_1 0\rangle\langle smJ-m\mid l_2 0\rangle\\&\times(\delta_{\alpha'\alpha}\delta_{s's}\delta_{l'l_1}-S^{J}_{\alpha's'l';\alpha sl_1})^*(\delta_{\alpha'\alpha}\delta_{s's}\delta_{l'l_2}-S^{J}_{\alpha's'l';\alpha sl_2})\ .\end{aligned} \tag{5}$$

The cross section for inelastic scattering ($\alpha'\neq\alpha, s'\neq s$) can be calculated from Eq. (5) as:

$$\sigma_{\alpha's';\alpha sm}^{\mathrm{inelastic}}=\frac{\pi}{k_\alpha^2}\sum_J(2J+1)\left\{\sum_{l'}\left|\sum_l\langle smJ-m\mid l0\rangle S^J_{\alpha's'l';\alpha sl}\right|^2\right\}\ . \tag{6}$$

The total reaction cross section is calculated from the $S$-matrix elements for elastic scattering ($\alpha'=\alpha, s'=s=\frac{3}{2}$) as

$$\sigma_{\alpha s;\alpha sm}^{\mathrm{reaction}}=\frac{\pi}{k_\alpha^2}\sum_{J\geq|m|}(2J+1)\left\{1-\sum_{l'}\left|\sum_l\langle smJ-m\mid l0\rangle S^J_{\alpha sl';\alpha sl}\right|^2\right\}\ . \tag{7}$$

We note that in both (6) and (7) $l$ enters coherently, but $l'$ enters incoherently. For the total reaction cross section the partial cross sections are restricted to $J\geq|m|$, because the "1" in Eq. (7) is due to

$$\sum_l\langle smJ-m\mid l0\rangle^2=1$$

for $J\geq|m|$. For $J=\frac{1}{2}$ and $|m|=\frac{3}{2}$ all partial cross sections are zero.

From Eqs. (4), (6), and (7) the tensor analyzing power for fusion $T_{20}^{\mathrm{fus}}$ can be calculated according to Eq. (1), and the cross section for fusion from Eqs. (4), (6), and (7) as

$$\sigma^{\text{fus}} \equiv \sigma^{\text{fus}}_{\alpha s} = \frac{1}{2s+1} \sum_{m=-s}^{+s} \sigma^{\text{fus}}_{\alpha s m} \ .$$

In the detailed calculations (see the following section) only inelastic excitations of the $^{23}$Na projectile to its $\frac{5}{2}^+$ and $\frac{7}{2}^+$ excited states and target excitation to the $2^+$ state were considered.

## V. DISCUSSION

In this section we will now investigate whether ground state properties (spectroscopic deformation of $^{23}$Na) and additional coupling to excited states of the projectile and/or target are able to describe the cross section *and* the tensor analyzing power for sub-barrier fusion of $^{23}$Na with $^{48}$Ti and $^{206}$Pb. Calculations were performed using the formalism described in the preceding section with the nuclear potential parameters listed in Table II. The $S$-matrix elements needed for the calculation of $\sigma^{\text{fus}}$ and $T^{\text{fus}}_{20}$ were calculated with the coupled-channels code ECIS79.[33] In these calculations the Coulomb radius was taken to be $R_C = 1.2(A_P^{1/3} + A_T^{1/3})$ fm. It is sufficient to perform these calculations with maximum $J$ values of $J_{\max} = 39.5\hbar$ (lowest energies) to $79.5\hbar$ (highest energies) because only "low" partial waves contribute to fusion (see also Fig. 7). Various tests assured us that the choice of $J_{\max}$ does not affect the results for $\sigma^{\text{fus}}$ and for $T^{\text{fus}}_{20}$. For all coupling schemes only $E2$ transitions were considered. The nuclear form factors for reorientation and inelastic excitation were chosen to be proportional to the first derivative of the nuclear potentials. Furthermore, the usual Coulomb form factors for $E2$ transitions were used for inelastic excitations and reorientation coupling. Experimental $B(E2)$ values and excitation energies are collected in Table III.

The results of these calculations for $\sigma^{\text{fus}}$ and $T^{\text{fus}}_{20}$ are shown in Fig. 4 together with a pictorial description of the various coupling schemes and their related symbols to mark the calculations. The dotted curves in the upper part of the figure represent as a reference a one-dimensional calculation for $\sigma^{\text{fus}}$ which is restricted to the elastic channel only (i.e., without deformation). As expected, this calculation reproduces the measured cross section for fusion at above-barrier energies well, but underpredicts it significantly at sub-barrier energies. This one-dimensional calculation necessarily predicts zero values for $T^{\text{fus}}_{20}$. When aligned projectiles are considered, the spectroscopic deformation of $^{23}$Na must be included in the coupled-channels analysis. This was achieved by calculating the matrix elements of the reorientation coupling in the ground state of the $^{23}$Na projectile. This reorientation matrix element is proportional to the spectroscopic quadrupole moment of $^{23}$Na.

TABLE III. $B(E2)$ values and excitation energies.

| Coupling process | $E^*$ (MeV) | $B(E2)$ ($e^2$ fm$^4$) |
|---|---|---|
| $^{23}$Na: $I=\frac{3}{2} \rightarrow I'=\frac{5}{2}$ | 0.44 | 157[a] |
| $^{23}$Na: $I=\frac{3}{2} \rightarrow I'=\frac{7}{2}$ | 2.08 | 73[a] |
| $^{48}$Ti: $I=0 \rightarrow I'=2$ | 0.98 | 720[b] |
| $^{206}$Pb: $I=0 \rightarrow I'=2$ | 0.80 | 910[c] |

[a]Reference 35.
[b]Reference 36.
[c]Reference 37.

With the spectroscopic deformation included in the calculations for $\sigma^{\text{fus}}$, only a slight enhancement at energies below the barrier and nearly the same results at energies above the barrier were observed. For $T^{\text{fus}}_{20}$ the deformation produces a large tensor analyzing power below the barrier, in particular for the $^{23}$Na+$^{206}$Pb system, reflecting the strong influence of the spectroscopic deformation of the projectile on the fusion process (solid curves in the bottom part of Fig. 4). While the experimental fusion cross section is still underestimated by these calculations, they overpredict the measured tensor analyzing power for fusion. Additional degrees of freedom should increase the fusion cross section at energies below the barrier and decrease the tensor analyzing power for fusion.

Thus, various coupled-channels calculations have been performed including coupling to excited states of the projectile and/or target. The short-dashed curve in Fig. 4 takes into account reorientation coupling in the ground state of $^{23}$Na and coupling to its first excited $\frac{5}{2}^+$ state. The additional coupling to the second excited $\frac{7}{2}^+$ state is marked by the long-dashed curves. Finally, the additional coupling to the $2^+$ state of the $^{48}$Ti target is shown as a long-dashed–short-dashed curve. As a result of these calculations the cross section for fusion is indeed increased gradually at sub-barrier energies, whereas $T^{\text{fus}}_{20}$ decreases. This is more pronounced for the $^{23}$Na + $^{206}$Pb system. The target excitation for $^{206}$Pb is negligible, whereas projectile and target excitation contribute about equally in the $^{23}$Na+$^{48}$Ti system (see below). For $\sigma^{\text{fus}}$ only the results of the calculations for the most complex coupling schemes (long-dashed curve for $^{23}$Na+$^{206}$Pb, long-dashed–short-dashed curve for $^{23}$Na + $^{48}$Ti) are shown because there are only minor differences between this result and the results for the other coupling schemes. On the other hand, the influence of these inelastic channels on the sub-barrier fusion process is more pronounced in $T^{\text{fus}}_{20}$, as shown in the bottom part of Fig. 4.

The data for $T^{\text{fus}}_{20}$ are well reproduced by the calculations with the most complex coupling scheme shown in Fig. 4. But these excited states still cannot account for the measured fusion cross sections at energies below the barrier. Within the $K=\frac{3}{2}$ ground state rotational band of $^{23}$Na there are no more allowed ground state $E2$ transitions. Only multistep processes or (electric) transitions with multipolarities higher than $\lambda=2$ are possible. The next level in the $^{48}$Ti target nucleus (the $4^+$ state at 2.3 MeV excitation energy) could be excited only through $E4$ transitions or through a two-step process. It is not expected that the inclusion of such processes will change our result significantly. This expectation is also supported by semiclassical calculations[38] which investigate the influence of other inelastic channels or reorientation coupling of excited states. These calculations provide a description of the fusion process with aligned $^{23}$Na projectiles which are in good agreement with the results

from the quantum-mechanical coupled-channels calculations.[38]

The different enhancements of the sub-barrier fusion cross section for both systems and the reduction of $T_{20}^{\text{fus}}$ when coupling is included can be understood qualitatively in the following way. It follows from general arguments[4] that coupling of additional degrees of freedom to the one-dimensional motion will enhance the fusion probability of the system through the splitting of the central potential and thus through the splitting of the barrier. The alignment of $^{23}$Na serves as such an additional degree of freedom. Therefore, the barrier is split due to the $m=\frac{3}{2}$ and $m=\frac{1}{2}$ magnetic substrates. This is illustrated in Fig. 8. For $^{23}$Na projectiles in the $m=\frac{3}{2}$ magnetic substate, the barrier is lower than the barrier for an unpolarized beam. For the $m=\frac{1}{2}$ component the barrier is higher. Furthermore, the additional coupling to excited states leads to a splitting of the corresponding $m=\frac{3}{2}$ and $m=\frac{1}{2}$ barriers.

The "sub-barrier enhancement" of the fusion cross section can be estimated from the change in barrier height $F_B$ caused by the barrier splitting. Because we are only interested in a qualitative understanding of the barrier splitting, the "constant coupling limit" was used[39] to evaluate the coupling strength $F_B$ at the radial position $R_B$ of the barrier

$$F_B=\frac{1}{\sqrt{4\pi}}\left[-\beta R\frac{dV_{\text{nucl}}(r)}{dr}+\frac{3Z_PZ_Te^2\beta R^2}{5r^3}\right]\Bigg|_{r=R_B}.$$

We use $R=1.2A^{1/3}$ and $\beta$ values calculated from the experimental $B(E2)$ values. For $V_{\text{nucl}}(r)$ the potential parameters from Table II (real part) were used.

For inelastic excitation of the projectile and target one obtains the following for $^{23}$Na+$^{48}$Ti: $F_B=-1.7$ MeV ($\frac{5}{2}^+$), $-1.5$ MeV ($\frac{7}{2}^+$), and $-0.9$ MeV ($2^+$). For $^{23}$Na+$^{206}$Pb one obtains $F_B=-4.0$ MeV ($\frac{5}{2}^+$), $-3.7$ MeV ($\frac{7}{2}^+$), and $-0.3$ MeV ($2^+$). These values clearly indicate the points discussed before:

(i) The coupling strength for projectile excitation is about 2 to 3 times larger for the target with the larger $Z$ value ($^{206}$Pb) as compared to the one with the smaller $Z$ value ($^{48}$Ti) which leads to a larger enhancement of $\sigma^{\text{fus}}$ for $^{23}$Na + $^{206}$Pb at sub-barrier energies.

(ii) Both excited states of the projectile must be considered.

(iii) Target excitation is almost negligible for the $^{206}$Pb target, whereas it has to be included in the $^{23}$Na+$^{48}$Ti analysis.

To explain the reduction of $T_{20}^{\text{fus}}$ when coupling to excited states is included, we consider the data point $T_{20}^{\text{fus}}\approx 0.8$ at 108 MeV bombarding energy for $^{23}$Na + $^{206}$Pb. Without coupling to excited states, only the $m=\frac{3}{2}$ barrier is important for fusion. The barrier corresponding to $m=\frac{1}{2}$ is too high to obtain a considerable fusion probability. But with coupling to excited states some of the "new" $m=\frac{1}{2}$ barriers are lowered (see Fig. 8), increasing the fusion probability for $m=\frac{1}{2}$. The same holds for $m=\frac{3}{2}$. But the fusion cross section for $m=\frac{1}{2}$ increases more than for $m=\frac{3}{2}$. This is shown in Fig. 9, where partial cross sections for fusion are compared for the $m=\frac{3}{2}$ and $m=\frac{1}{2}$ magnetic substates. As a reference, the calculation of the reorientation coupling in the ground state of $^{23}$Na is shown as a solid curve (coupling scheme $\alpha$). (Note that lower case script letters appear as circled letters in the figure.) The additional coupling to excited states of the projectile (coupling scheme $\mathcal{A}$) is marked by the dashed curve. From these calculations one obtains the ratios of the fusion cross sections for the same magnetic substate, but for different coupling schemes, $\sigma^{\text{fus},\mathcal{A}}_{m=1/2}/\sigma^{\text{fus},\alpha}_{m=1/2}=7.3$ and $\sigma^{\text{fus},\mathcal{A}}_{m=3/2}/\sigma^{\text{fus},\alpha}_{m=3/2}=3.7$. This larger increase for $m=\frac{1}{2}$ than for $m=\frac{3}{2}$, relative to the ground state reorientation coupling, results in the decrease of $T_{20}^{\text{fus}}$ when coupling to excited states is included. (Of course, the absolute fusion cross section for $m=\frac{3}{2}$ is larger than for $m=\frac{1}{2}$.)

Despite the fact that the data for $T_{20}^{\text{fus}}$ are well fitted, we fail to reproduce the fusion cross section at sub-barrier energies. In the frame of the model employed here, transfer channels which couple to the fusion chan-

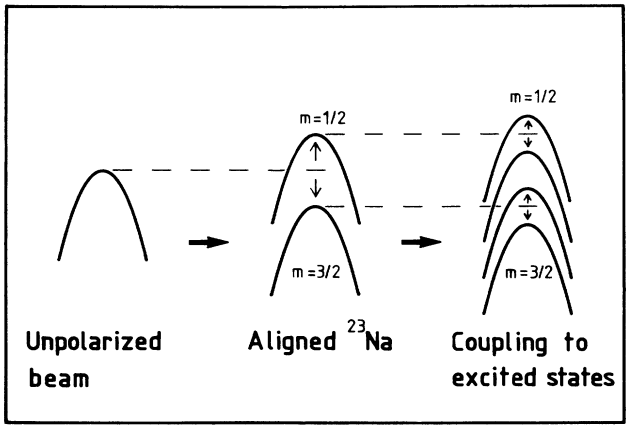


FIG. 8. Schematic picture of barrier splitting for an aligned $^{23}$Na beam (see the text).

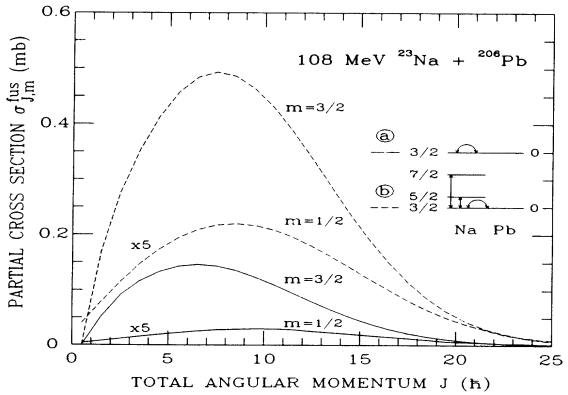


FIG. 9. Partial fusion cross sections for 108 MeV $^{23}$Na + $^{206}$Pb for different magnetic substates. The curves for $m=\frac{1}{2}$ are multiplied by a factor of 5 for a better visual representation. Note that the partial fusion cross section vanishes for $J=\frac{1}{2}$ and $m=\frac{3}{2}$.

TABLE IV. Effective ground state $Q$ values (in MeV) for one- and two-nucleon transfer for the systems $^{23}Na+^{48}Ti$ and $^{23}Na+^{206}Pb$, according to $Q_{eff}=Q_{g.s.}+(V_C^{initial}-V_C^{final})$. $Q_{g.s.}$ denotes the ground state $Q$ value and $V_C$ denotes the height of the Coulomb barrier calculated according to Ref. 12.

| | $^{23}Na+^{48}Ti$ | $^{23}Na+^{206}Pb$ |
|---|---|---|
| 1p stripping | −0.3 | +3.5 |
| 2p stripping | −4.0 | +1.9 |
| 1n stripping | −4.3 | −5.7 |
| 2n stripping | −4.4 | −9.4 |
| 1p pickup | −1.2 | −4.6 |
| 2p pickup | −8.5 | −16.5 |
| 1n pickup | −4.7 | −1.1 |
| 2n pickup | −4.5 | +1.2 |

nel should be considered. Recent work on this topic has shown[40–43] that transfer reactions can strongly influence the cross section for fusion at energies below the barrier. Table IV shows the ground state $Q$ values (corrected for the change in Coulomb energy for charged particle transfer) for one- and two-nucleon transfer. All $Q$ values are negative for $^{23}Na+^{48}Ti$, whereas for the heavy system $^{23}Na+^{206}Pb$ both positive and negative $Q$ values are present. From both ($Q<0, Q>0$) types of transfer reactions significant contributions to $\sigma^{fus}$ could be expected.[40,41,43] However, it is an open question whether the total transfer strength[42] or specific $Q$ value channels[43] are responsible for the larger fusion probabilities at sub-barrier energies.

Since $T_{20}^{fus}$ is already explained by coupling to inelastic channels, the influence of transfer channels must fulfill a stringent constraint: this additional degree of freedom has to raise the sub-barrier fusion cross section, but it must not change the predictions for the tensor analyzing power for fusion $T_{20}^{fus}$ (see Fig. 4).

## VI. SUMMARY AND CONCLUSION

Cross sections and tensor analyzing powers for fusion were measured for two heavy ion systems: $^{23}Na+^{48}Ti$ and $^{23}Na+^{206}Pb$. Aligned heavy ions offer new possibilities to study the sub-barrier fusion process by measuring not only the fusion cross section but also the tensor analyzing power for fusion which serves as a new independent entrance channel observable.

As expected for heavy ion systems, the fusion excitation functions cannot be reproduced at sub-barrier energies by a one-dimensional barrier penetration model. In this low energy regime large tensor analyzing powers for fusion are observed for both systems. This can be attributed mainly to the strong influence of the spectroscopic deformation of $^{23}Na$. However, the comparison of the experimental data with coupled-channels calculations shows that consideration of the ground state properties of the projectile and the target alone is not enough to describe $\sigma^{fus}$ *and* $T_{20}^{fus}$. At sub-barrier energies $\sigma^{fus}$ is underpredicted and $T_{20}^{fus}$ is overpredicted by these calculations. In addition to the spectroscopic deformation, we are forced to include further degrees of freedom which (i) have to raise the fusion cross section at sub-barrier energies, and (ii) have to decrease the tensor analyzing power for fusion.

It was shown that coupling to excited states of the projectile and target satisfies both conditions which could be understood qualitatively within the intuitive picture of barrier splitting caused by the coupling mechanism.[4]

The experimental data for the tensor analyzing power for fusion can be described within this model. This result shows the important role of entrance channel effects via the deformation of the projectile and of inelastic excitations of the reaction partners in the low energy regime of the sub-barrier fusion between massive heavy ions. Furthermore, it was shown that the tensor analyzing power for fusion is more sensitive to these degrees of freedom than the fusion cross section.

However, the enhancement of the fusion cross section for both systems at sub-barrier energies cannot be reproduced by the coupled-channels calculations. This failure may be interpreted as the need to include transfer channels. Similar observations have been reported in the $^{12}C+^{48}Ti$ reaction[44] in which the cross section for inelastic scattering could be well described by coupled-channels calculations, but not the corresponding fusion cross section at sub-barrier energies. It certainly would be desirable to have a full quantum-mechanical coupled-channels calculation for spin-$\frac{3}{2}$ particles including inelastic excitations and transfer reactions taking into account finite range and recoil effects.

As was pointed out recently by Nagarajan, Mahaux, and Satchler,[45] such coupling effects can also be studied in a somewhat more phenomenological way by using an energy dependent optical potential obtained from elastic scattering using dispersion relations. Recently, Franzin and Hussein have adopted such a dispersion relation to sub-barrier fusion reactions.[46] Elastic scattering experiments with aligned $^{23}Na$ ions are now under way[47] to check the applicability of this approach.

## ACKNOWLEDGMENTS

We are grateful to G. Grawert and K. Heck for many helpful discussions. We also thank E. Jaeschke and R. Repnow for their technical assistance in preparing the decelerated beam. One of us (P.P.) was the recipient of an Alexander von Humboldt Award. This work was partly supported by the Bundesministerium für Forschung und Technologie, Bonn, under Contract No. 06 MR 853.

*Present address: Department of Physics, State University of New York at Stony Brook, Stony Brook, NY 11794.

†Present address: BASF AG, D-6700 Ludwigshafen, Federal Republic of Germany.

‡Present address: Department of Physics, The University of Birmingham, Birmingham B15 2TT, England.

§Present address: Siemens AG, D-8000 München, Federal Republic of Germany.

[1]N. Fröman and P. O. Fröman, *JWKB Approximation* (North-Holland, Amsterdam, 1965); D. L. Hill and J. A. Wheeler, Phys. Rev. **89**, 1102 (1953).
[2]M. Beckerman, Phys. Rep. **129**, 145 (1985), and references therein.
[3]*Proceedings of the International Conference on Fusion Reactions below the Coulomb Barrier,* Vol. 219 of *Lecture Notes in Physics,* edited by S. G. Steadman (Springer, Heidelberg, 1985), and references therein.
[4]C. H. Dasso, S. Landowne, and A. Winther, Nucl. Phys. **A405**, 381 (1983); **A407**, 221 (1983).
[5]K.-H. Möbius *et al.*, Phys. Rev. Lett. **46**, 1064 (1981); K.-H. Möbius *et al.*, Z. Phys. A **306**, 335 (1982); **310**, 159 (1983).
[6]P. Egelhof *et al.*, Phys. Rev. Lett. **44**, 1380 (1980); A Weller *et al.*, *ibid.* **55**, 480 (1985).
[7]D. Krämer *et al.*, Nucl. Instrum. Methods **220**, 123 (1984).
[8]D. Fick, Annu. Rev. Nucl. Part. Sci. **31**, 53 (1981); M. Simonius, in *Polarization Nuclear Physics,* Vol. 30 of *Lecture Notes in Physics,* edited by D. Fick (Springer, Heidelberg, 1974).
[9]H. Jänsch, Ph.D. thesis, Philipps-Universität, 1985; H. Jänsch *et al.*, Nucl. Instrum. Methods **254**, 7 (1987).
[10]E. Steffens, Nucl. Instrum. Methods **184**, 173 (1981).
[11]W. Dreves *et al.*, Phys. Rev. Lett. **50**, 1759 (1983).
[12]L. C. Vaz, J. M. Alexander, and G. R. Satchler, Phys. Rep. **69**, 373 (1981).
[13]K.-H. Möbius and K. Blatt, Nucl. Instrum. Methods **225**, 293 (1984).
[14]B. Kolb, G. Hlawatsch, G. Rosner, Th. Walcher, H. Ingwersen, E. Jaeschke, and R. Repnow, Nucl. Instrum. Methods **188**, 555 (1981).
[15]G. Tungate *et al.*, J. Phys. G **12**, 1001 (1986).
[16]L. C. Vaz and J. M. Alexander, Phys. Rep. **97**, 1 (1983).
[17]A. Gavron, Phys. Rev. C **21**, 230 (1980).
[18]A. J. Sierk, Phys. Rev. C **33**, 2039 (1986).
[19]J. Tōke *et al.*, Nucl. Phys. **A440**, 327 (1985); B. B. Back *et al.*, Phys. Rev. C **32**, 195 (1985); R. Bock *et al.*, Nucl. Phys. **A388**, 334 (1982).
[20]K. Alder and A. Winther, *Electromagnetic Excitation* (North-Holland, Amsterdam, 1975).
[21]H. Leucker, Diploma thesis, Philipps-Universität, 1985.
[22]P. Zupranski *et al.*, Nucl. Instrum. Methods **167**, 193 (1979).
[23]V. E. Viola, K. Kwiatkowski, and M. Walker, Phys. Rev. C **31**, 1550 (1985).
[24]B. Jeckelmann, W. Beer, I. Beltrami, F. W. N. de Boer, G. de Chambrier, P. F. A. Goudsmit, J. Kern, H. J. Leisi, W. Ruckstuhl, and A. Vacchi, Nucl. Phys. **A408**, 495 (1983).
[25]H. H. Gutbrod, W. G. Winn, and M. Blann, Nucl. Phys. **A213**, 267 (1973).
[26]C. Y. Wong, Phys. Rev. Lett. **31**, 766 (1973).
[27]R. A. Broglia and A. Winther, in *Heavy Ion Reactions,* Vol. 52 of *Frontiers in Physics,* edited by D. Pines (Benjamin, Reading, 1981).
[28]R. Ö. Akyüz and A. Winther, in *Nuclear Structure and Heavy-Ion Collisions,* Proceedings of the International School of Physics "Enrico Fermi," Course LXXVII, Varenna, 1979, edited by R. A. Broglia, R. A. Ricci, and C. H. Dasso (North-Holland, Amsterdam, 1981).
[29]H. J. Krappe, J. R. Nix, and A. J. Sierk, Phys. Rev. C **20**, 992 (1979).
[30]J. Blocki, J. Randrup, W. J. Swiatecki, and C. F. Tsang, Ann. Phys. (N.Y.) **105**, 427 (1977).
[31]L. C. Vaz and J. M. Alexander, Phys. Rev. C **18**, 2152 (1978).
[32]M. J. Rhoades-Brown and P. Braun-Munzinger, Phys. Lett. **136B**, 19 (1984).
[33]J. Raynal, Phys. Rev C **23**, 2571 (1981).
[34]J. M. Blatt and L. C. Biedenharn, Rev. Mod. Phys. **24**, 258 (1952).
[35]D. Schwalm, E. K. Warburton, and J. W. Olness, Nucl. Phys. **A293**, 425 (1977).
[36]N. V. de Castro Faria, J. Charbonneau, J. l'Écuyer, and R. J. A. Lévesque, Nucl. Phys. **A174**, 37 (1971).
[37]J. L. Quebert, K. Nakai, R. M. Diamond, and F. S. Stephens, Nucl. Phys. **A150**, 68 (1970).
[38]K.-H. Möbius and G. Grawert, see Ref. 3, p. 305; D. Mukhopadhyay, K.-H. Möbius, K. Heck, and G. Grawert, Phys. Rev. C **35**, 1324 (1987).
[39]R. Lindsay and N. Rowley, J. Phys. G **10**, 805 (1984).
[40]K. E. Rehm, F. L. H. Wolfs, A. M. van den Berg, and W. Henning, Phys. Rev. Lett. **55**, 280 (1985).
[41]J. Wiggins, R. Brooks, M. Beckermann, S. B. Gazes, L. Grodzins, A. P. Smith, S. G. Steadman, and Y. Xiao, Phys. Rev. C **31**, 1315 (1985).
[42]W. Henning, F. L. H. Wolfs, J. P. Schiffer, and K. E. Rehm, Phys. Rev. Lett. **58**, 318 (1987).
[43]R. A. Broglia, C. H. Dasso, S. Landowne, and A. Winther, Phys. Rev. C **27**, 2433 (1983); S. Landowne, S. C. Pieper, and F. Videbaek, *ibid.* **35**, 597 (1987).
[44]D. M. de Castro Rizzo and N. Alamanos, Nucl. Phys. **A443**, 525 (1985).
[45]M. A. Nagarajan, C. C. Mahaux, and G. R. Satchler, Phys. Rev. Lett. **54**, 1136 (1985).
[46]V. L. M. Franzin and M. S. Hussein, University of São Paulo Report IFUSP/P-596, 1986.
[47]H. Leucker (private communication).